Data Assimilation for Orszag-Tang Magnetohydrodynamic Vortex Problem

Jinsu Kim
Dept. Mechanical and Aerospace Engineering
Princeton University
jk9075@princeton.edu

***Abstract*—This project investigates the application of the Ensemble Kalman Filter (EnKF), a data assimilation method based on Monte-Carlo approximation, to estimate the dynamics of a two-dimensional Magnetohydrodynamic (MHD) turbulent phenomenon called Orszag-Tang vortex. The Orszag-Tang vortex has been widely studied to understand the small-scale turbulent structure from the nonlinear interaction between the magnetic field and plasma. The EnKF is adapted to estimate the nonlinear dynamics of the MHD vortex under the uncertainties arising from the measurement and process errors in the MHD system. We verify the possibilities and limitations of the EnKF for estimating the state in nonlinear MHD turbulence structure.**

***Index Terms*—Ensemble Kalman Filter, Magnetohydrodynamics, Orszag-Tang Vortex**

I. Introduction

A plasma is a fourth state of matter that consists of ionized particles such as ions, electrons, and neutrals. It behaves like an electrically conducting fluid [1] interacting with self-consistent and external electromagnetic fields. Due to its complex dynamics, accurate prediction of the plasma dynamics has been highlighted in several areas, ranging from laboratory fusion experiments to space weather forecasting. In real plasma systems, however, the observational data differ from model predictions due to measurement and process errors. This uncertainty necessitates a data assimilation framework to integrate the data into the physical models and improve the accuracy of state estimation.

In this project, we utilize one of the data assimilation methods based on Monte-Carlo approximation called Ensemble Kalman Filter (EnKF), to estimate the dynamics of a two-dimensional Magnetohydrodynamic system with a good example of the turbulent phenomenon called Orszag-Tang vortex. The Orszag-Tang vortex problem shows the small-scale turbulent structure induced by the magnetic field's and plasma's nonlinear interaction. This is a benchmark for evaluating numerical methods in plasma physics. We integrate the MHD simulation with the EnKF algorithm to estimate the dynamics of the Orszag-Tang vortex from noisy measurements and partial observations. The use of the EnKF is motivated by the fact that the integration of the Monte-Carlo method enables the reduction of the computation to estimate the error covariance by using a small ensemble of samples. This is suited for both high-dimensional and nonlinear systems with difficulties in linearizing the dynamic models, including MHD systems.

We will introduce the governing equations of MHD to describe the dynamics of MHD systems and conditions for the Orszag-Tang vortex problem. Then, we will cover the theoretical foundation of the Ensemble Kalman Filter and how to apply this method to recover the system's dynamics from noisy and partial observations. We will represent the numerical results and discuss the validity of the EnKF in estimating the MHD turbulence under uncertainty.

II. Background

A. Magnetohydrodynamics

Magnetohydrodynamics (MHD) is one of the well-known models, which assumes that the plasma is a single fluid linearly combined with the average motions of individual species based on charge-neutrality and small gyro-radius approximations. This can describe the equilibrium and large-scale dynamics of the magnetized plasma. The governing equations of MHD are derived by coupling the fluid equations with Maxwell's equations. Here, ρ, u, p are the fluid variables, corresponding to average mass density, drift velocity, and thermal pressure. E, B, and J are the electromagnetic variables, where E and B are the electric and magnetic fields, respectively, and J is the current density of the plasma.

The fluid variables are governed by Equation 1, 2, and 3, which correspond to continuity, momentum, and adiabatic equations, respectively.

$$\frac{\partial \rho}{\partial t} + \nabla \cdot (\rho u) = 0 \tag{1}$$

$$\rho \frac{du}{dt} = -\nabla p + \frac{J \times B}{c} \tag{2}$$

$$\frac{d}{dt}\left(\frac{p}{\rho^{\gamma}}\right) = 0 \tag{3}$$

On the other hand, E,B,and J are governed by Equation 4, 5, 6, and 7, which correspond to Ampere's law, Ohm's law, Gauss' law, and Faraday's law.

$$J = \frac{c}{4\pi} \nabla \times B \tag{4}$$

$$E + \frac{u \times B}{c} = \eta J \tag{5}$$

$$\nabla \cdot B = 0 \tag{6}$$

$$\nabla \times E = -\frac{1}{c}\frac{\partial B}{\partial t} \tag{7}$$

This self-consistent system can be simplified as Equation 8 by assuming the ideal MHD, where the resistivity η is 0 so that the magnetic flux is now conserved.

$$\begin{aligned} \frac{\partial \rho}{\partial t} + \nabla \cdot (\rho u) &= 0 \\ \rho \frac{du}{dt} = -\nabla p + \frac{1}{4\pi}(\nabla \times B) \times B \\ \frac{d}{dt}(\frac{p}{\rho^\gamma}) &= 0 \\ \nabla \cdot B &= 0 \\ \frac{\partial B}{\partial t} &= \nabla \times (u \times B) \end{aligned} \tag{8}$$

We will cover this ideal MHD system described by the variables ρ, u, p, and B. Note that Equation 6 must be satisfied during the simulation, while the conservation laws corresponding to the mass, momentum, and total energy are also satisfied. We simulate the MHD vortex with the Constrained Transport Method [2], implemented within the framework of the finite volume method to preserve the divergence-free condition.

B. Orszag-Tang MHD vortex

A supersonic MHD turbulence model problem known as Orszag-Tang MHD vortex [3] is observed in a two-dimensional periodic system. There is a transition to MHD turbulence when the sinusoidal perturbations in the velocity and magnetic field are applied as Equation 9. It is known that the nonlinear interaction between the fluid motion of the plasma and the magnetic field leads to the small-scale turbulent structure [3]

$$\begin{aligned} v &= -\sin y\hat{x} + \sin x\hat{y} \\ B &= -\sin y\hat{x} + \sin 2x\hat{y} \end{aligned} \tag{9}$$

Figure 1 shows the evolution of the magnetic pressure and vorticity with the initial perturbation mentioned above. In this figure, we can observe that the complex interaction induces the shock formulation at different speed regimes [4]. This MHD vortex has been used in several studies to evaluate the performance of the numerical codes at handling the formation of MHD shocks while preserving the divergence-free condition. We also utilize this problem to verify the effectiveness of the EnKF.

III. Methodologies

A. Kalman Filter

The Kalman filter [5] is an approach to estimate the state variables with uncertainties based on the Markov chain and Gaussian estimation. The dynamic system perturbed by the process (or model) and measurement noises can be estimated using the measurement data and Gaussian estimation. Consider the discrete-time dynamical system, which is described

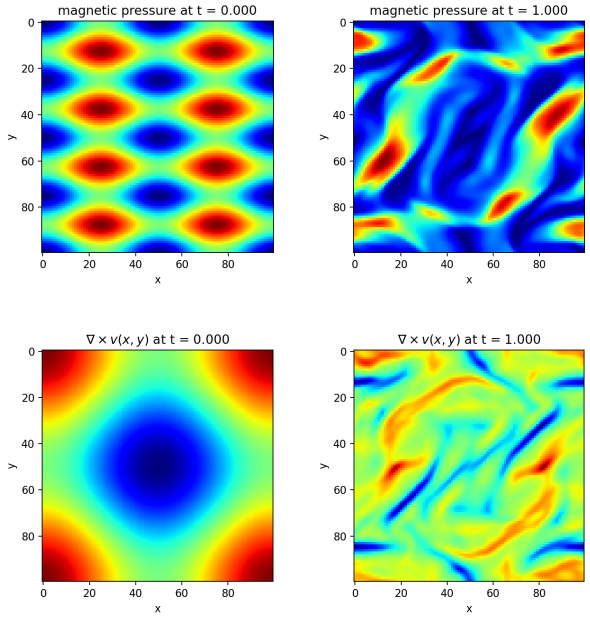

Fig. 1: The evolution of magnetic pressure and vorticity in 2D Orszag-Tang MHD vortex

as Equation 10. In this system, ζ_k and η_k are model and measurement error, respectively.

$$\begin{aligned} X_{k+1} &= f(X_k) + \zeta_k \\ Y_{k+1} &= h(X_{k+1}) + \eta_k \end{aligned} \tag{10}$$

The initial state and errors follow the Gaussian: $X_0 \sim N(\mu_0, \Sigma_0)$, $\zeta_k \sim N(0, \Sigma_x)$ and $\eta_k \sim N(0, \Sigma_y)$. Also, the i.i.d property is satisfied for the error (ζ_k) and (η_k). Then, for the linear system where $f(X_k) = FX_k$, the estimation of the system's state considering the existence of the noise is now possible by using a series of observed data with a Bayesian rule.

First, μ_k and Σ_k, the posterior of the mean and covariance of the state at time step k, respectively, are described in Equation 11 and 12.

$$\mu_{k+1} = \hat{\mu}_{k+1} + K_{k+1}(Y_{k+1} - H\hat{\mu}_{k+1}) \tag{11}$$

$$\Sigma_{k+1} = (I - K_{k+1}H)\hat{\Sigma}_{k+1} \tag{12}$$

where K_k is a kalman gain at time step k, defined as Equation 13.

$$K_{k+1} = \hat{\Sigma}_{k+1}H^T(\Sigma_y + H\hat{\Sigma}_{k+1}H^T)^{-1} \tag{13}$$

The prediction of the next prior mean and covariance $\hat{\mu}_k$ and $\hat{\Sigma}_k$ at time step t, is obtained by Equation 14 and Equation 15.

$$\hat{\mu}_{k+1} = F\mu_k \tag{14}$$

$$\hat{\Sigma}_{k+1} = F\Sigma_k F^T + \Sigma_x \tag{15}$$

For the nonlinear dynamic system, the variation of the Kalman Filter called Extended Kalman Filter (EKF) can be applied by computing the Jacobian of $f(X_k)$ to linearize the dynamics. However, it is difficult to express the explicit formula in MHD dynamics. Thus, we will instead use the alternative called the Ensemble Kalman Filter (EnKF).

B. Ensemble Kalman Filter

Ensemble Kalman Filter(EnKF) is a Monte Carlo method-based Kalman filtering [6], replacing the covariance required for Kalman updating by the sample covariance of the ensemble. EnKF can be a good choice for MHD since it does not require linearization for nonlinear dynamics approximation by ensemble sampling. Instead of evolving the mean and covariance matrix from the original state for each time step, the EnKF uses an ensemble of model states to approximate the covariance matrix. The state vector X_k and measurement Y_k are now collected as a part of the ensemble X_k^e and Y_k^e, where $X_k^e = [X_k^1, X_k^2, ...X_k^n]$ and $Y_k^e = [Y_k^1, Y_k^2, ...Y_k^n]$ with the size of the ensemble n. Each column represents the unweighted sample obtained from the prior distribution at k time step.

Again, the mean and covariance of the state distribution are now computed by empirical mean $\hat{\mu}_{x,k}^e$ and covariance $\hat{\Sigma}_{x,k}^e$ following Equation 16 and 17.

$$\hat{\mu}_{x,k}^e = E[X_k^e] = \frac{1}{n}\sum_{i=1}^{n} x_k^i \tag{16}$$

$$\hat{\Sigma}_{x,k}^e = cov[X_k^e] = \frac{(X_k^e - \hat{\mu}_{x,k}^e)(X_k^e - \hat{\mu}_{x,k}^e)^T}{n-1} \tag{17}$$

Then, the posterior ensemble X_{k+1}^e updated by the new ensemble measurement Y_{k+1}^e can be written as Equation 18. Here, Y_{k+1}^e is the ensemble measurement by sampling from the multivariate Gaussian distribution of the covariance Σ_y at $k+1$ time step.

$$X_{k+1}^e = \hat{X}_{k+1}^e + K_{k+1}^e(Y_{k+1}^e - H\hat{X}_{k+1}^e) \tag{18}$$

Note that it is not necessary to compute the posterior covariance like Equation 12 to get the Kalman gain K_{k+1}^e. Instead, using Equation 19 with empirical covariance gives us K_{k+1}^e.

$$K_{k+1}^e = \hat{\Sigma}_{x,k+1}^e H^T(\Sigma_y + H\hat{\Sigma}_{x,k+1}^e H^T)^{-1} \tag{19}$$

For each time step, the ensemble state prediction $\hat{X}_{k+1}^e$ is computed by $\hat{X}_{k+1}^e = f(X_k^e)$, which will be used again for the next posterior ensemble state X_{k+1}^e via Equation 18 with the new kalman gain described as Equation 19. The detailed implementation of EnKF for MHD vortex simulation will be covered in the next section.

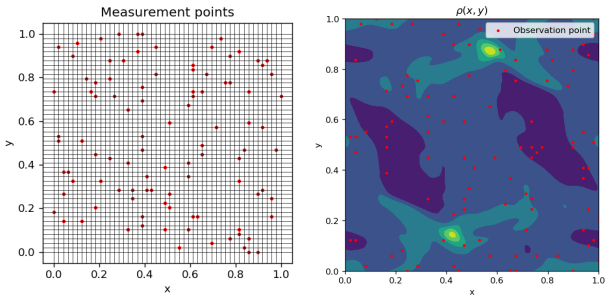

Fig. 2: Distribution of the measurement points on the mesh grid for EnKF

C. Application of EnKF for MHD simulation

The MHD system described in the previous section can be represented as Equation 10, where $X_k = [\rho, u_x, u_y, P, B_x, B_y]$ and $\rho, u_x, u_y, p, B_x, B_y \in R^{N_g \times N_g}$, where N_g is the number of the mesh grid. Then, $f(X)$ gives us the next state X_{k+1} by solving the ideal MHD equations in the conservative form as seen in Equation 8. Since the ideal MHD system assumes low-frequency and large-scale behavior while ignoring the kinetic effect, there is a limitation in describing the exact dynamics in a real system. The process error, also called the model error, should be considered. Thus, we added the model error ζ_k, which is sampled from the multivariate Gaussian distribution $N(0, \Sigma_x)$. Besides, observing the physical quantities in MHD systems, the lack of information about initial and boundary conditions often results in noisy measurements. Therefore, the measurement error η_k, which follows the multivariate Gaussian distribution $N(0, \Sigma_y)$, is also added for each time step. Next, Y_k is the output vector obtained from the measurement points, which is represented as $[\tilde{\rho}, \tilde{u}_x, \tilde{u}_y, \tilde{p}, \tilde{B}_x, \tilde{B}_y]$ and $\tilde{\rho}, \tilde{u}_x, \tilde{u}_y, \tilde{p}, \tilde{B}_x, \tilde{B}_y \in R^{N_m}$, where N_m is the number of measurement points. The positions of the measurements are randomly given, which is represented in Figure 2. Figure 2 describes the coordinates of the measurement points on the mesh grid to measure the plasma density.

Our framework for the two-dimensional MHD turbulence simulation to estimate the dynamics under the uncertainties in the measurements and the model is described in Figure 3.

D. Simulation setup

The following setup for MHD transport simulation is described in Table I. Here, N_m is the number of mesh grid, T is the simulation time, L is the system's length, C_F is the Courant factor used for deciding the time difference for time integration, and dt_{min} is the minimum time difference for each time step. Note that dt is obtained by $dt = C_F \min \frac{\Delta x}{v_F + |v|}$ for the numerical stability during simulation, while v_F is the fast magnetosonic speed given as $v_F = \sqrt{v_A^2 + v_S^2}$. In addition, we applied the slope limit method [7] to avoid an abrupt increase in the gradient.

TABLE I: Setup for numerical MHD transport simulation

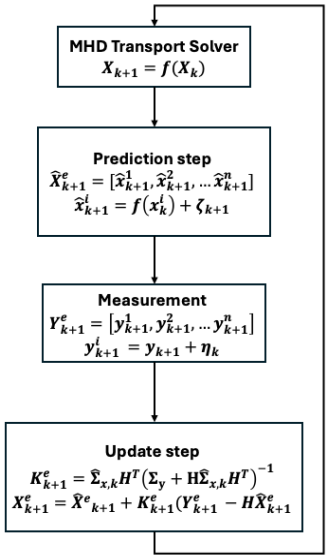

Fig. 3: The simplified framework for EnKF application to MHD turbulence dynamics estimation

N_m	T	L	C_F	dt_{min}
50	0.5(s)	1.0	0.25	0.001

The default parameters for the EnKF algorithm are given as Table II. Here, N_e, N_m, Σ_x, and Σ_y correspond to the ensemble size, the number of measurement points, the covariance of the model, and the measurement error. We originally planned to analyze the effect of the ensemble size, the number of measurement points, and the covariance of the noise. However, the EnKF application to MHD dynamics required numerical stability for computing the transport equation with respect to adding noise. Thus, we changed our project aim to check the validity of the EnKF application in the MHD turbulence structure. We just applied the EnKF algorithm with different parameters for each physical variable ρ, v_x, v_y, p, B_x, and B_y, following Table III, which describes the variables applied for the EnKF algorithm during simulation.

TABLE II: Default setting for EnKF parameters

N_e	N_m	Σ_x	Σ_y
100	100	0.01	0.01

TABLE III: List of variables applied for dynamics of the estimation

	Values
Variables	$[\rho,\ u_{x,y},\ p,\ B_{x,y}]$
N_e	100
N_m	100
$\Sigma_{x,y}$	[0.1, 0.01, 0.001, 0.0001]

IV. Numerical Results

In this section, we cover the EnKF application to estimate the dynamics of MHD turbulence while changing the variables following Table III. As mentioned, we added the Gaussian noise to the primitive variables $\rho, u_x, u_y, P, B_x, B_y$, respectively, and applied EnKF with the default parameter setting as Table II.

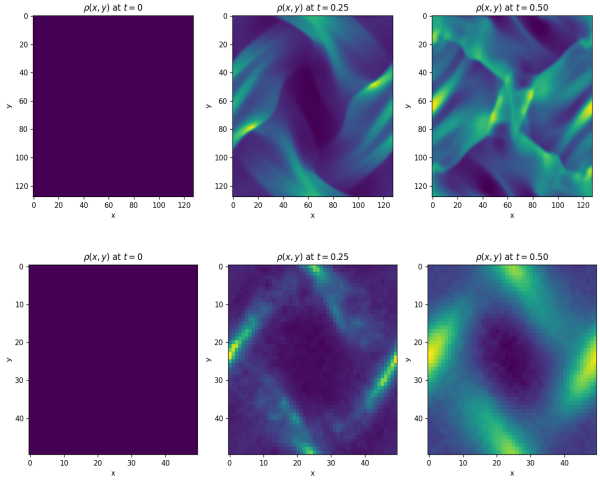

Fig. 4: The evolution of the plasma density during the simulation without noise (upper) and with noise (lower)

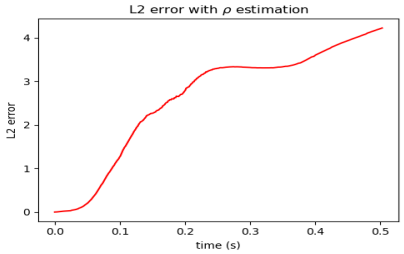

Fig. 5: L_2 norm error of the estimated plasma density over time

Here, we first added Gaussian noise to the plasma density for each prediction step. Figure 4 shows the evolution of the plasma density, while the upper one is the ground-truth result, and the lower one indicates the case where errors are considered following the setup as in Table II. In this figure, the turbulent structure, where the intersection of small-wave propagation, cannot be evolved when the EnKF is applied. Figure 5 describes the time evolution of the L_2 norm error of the plasma density, indicating that the difference increases over time. This means that the estimation of the dynamics results in the accumulation of errors over time due to the poor performance of the EnKF.

We estimated that the error added to the plasma density directly induces the offset of the small structure of the MHD turbulence. However, it seems that the scale of error does not affect the formation of the structure, which is supported by Figure 6. This implies that there is another factor resulting in the reduction of the turbulent structure.

Figure 7 shows the time evolution of the mean value of the divergence of the magnetic field during the simulation, and

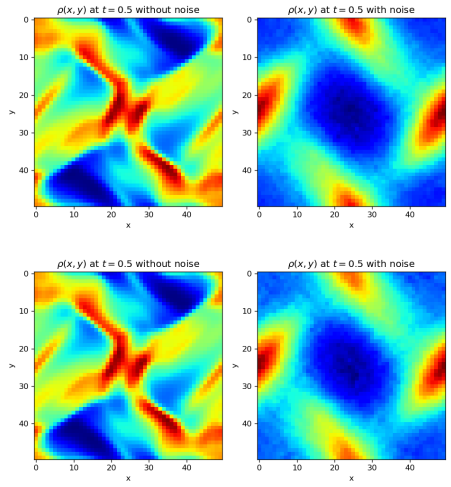

Fig. 6: Comparison of the final plasma density at $t = 0.5(s)$. The upper one is $\Sigma_x = \Sigma_y = 0.1$, and the bottom is $\Sigma_x = \Sigma_y = 0.0001$

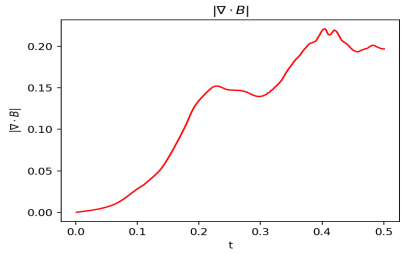

Fig. 7: Spatial average value of $|\nabla \cdot B|$ over time

Figure 8 represents the L_2 norm error of B over time. We can observe that the divergence of B increases over time, meaning that the transport solver does not satisfy the divergence-free condition. Since the original MHD transport solver uses the Constrained Transport Method to conserve the divergence-free condition, adding noise to the state vector X_k results in not only numerical instabilities but also a significant difference in the magnetic field structure. The reason for the violation of the divergence-free condition is estimated to be that the computation of the gradient with noisy data results in an

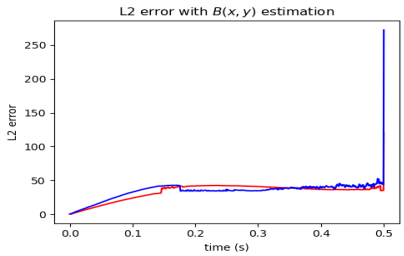

Fig. 8: L_2 norm error of the magnetic field estimation over time (Red line: Bx, Blue line: B_y)

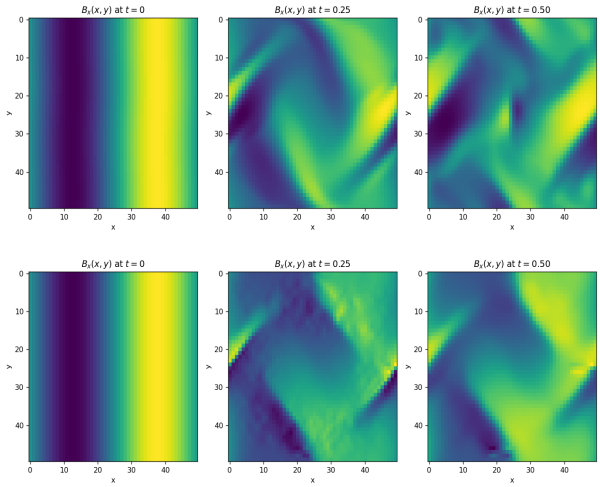

Fig. 9: Time evolution of B_x during the simulation without noise (upper) and with noise (lower) while $\Sigma_x = \Sigma_y = 0.0001$

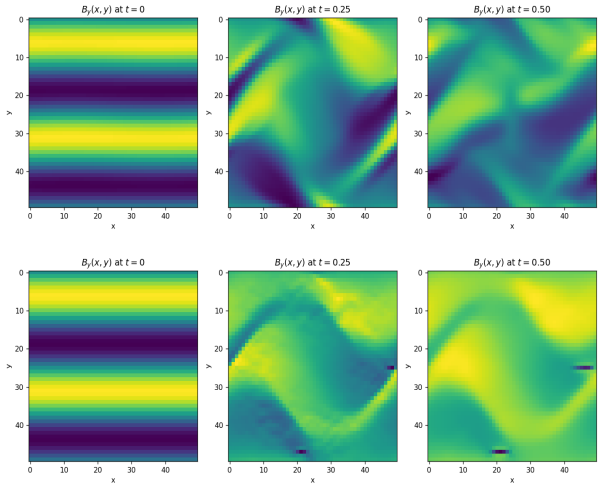

Fig. 10: Time evolution of B_y during the simulation without noise (upper) and with noise (lower) while $\Sigma_x = \Sigma_y = 0.0001$

abrupt increase in local points. This is supported by Figure 9 and 10, where the time evolution of the magnetic field is represented. From Figure 9, we can see that the shock formulation disappears when the noise is added. In Figure 10, the estimated B_y has a different structure from the ground-truth compared to the case of B_x, since the divergence-free condition is not satisfied by adding noise to the density.

We attempted to apply Gaussian noise to other variables u_x, u_y, B_x, and B_y in the same way as above; however, the MHD turbulence dynamics cannot be estimated, and numerical instabilities occurred during the simulation as shown in Figure 11. From Equation 8, the Ohm's law $\frac{\partial B}{\partial t} = \nabla \times (u \times B)$ shows the direct connection between the magnetic field and the drift velocity meaning that the noise from the velocity affects the time integration of the magnetic field. Thus, the Constrained Transport Method with added error terms may not conserve the divergence-free condition, eventually causing

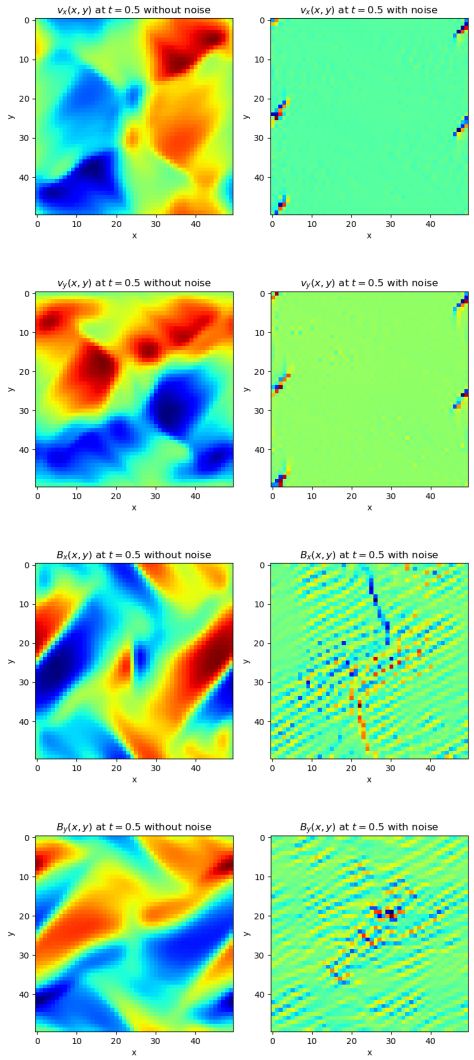

Fig. 11: Comparison of the u_x, u_y, B_x, and B_y at $t = 0.5(s)$ while adding noise with $\Sigma_x = \Sigma_y = 0.0001$.

numerical instabilities.

V. Conclusion

In this project, we integrated the MHD transport simulator with EnKF to estimate the dynamics under the uncertainties, considering the measurement noise and the lack of knowledge about the dynamics of the system. The use of EnKF can estimate the dynamics at the beginning of the simulation. However, the small structure of the MHD turbulence cannot be evolved via the EnKF application. Since the nonlinear interaction between the magnetic field and plasma induces this structure, estimating the magnetic field while satisfying the divergence-free condition is essential. Our analysis showed that the divergence-free condition and the magnetic field structure differed significantly from the ground-truth, and the noise scale was not the main factor. The issue is that the divergence-free condition is violated while adding noise during simulation. This has been shown from Figure 7, indicating that the equality constraint for divergence-free condition should be reflected in the filtering algorithm. The modification of the Kalman filter while conserving the equality constraints [8], [9] for the system can be considered. Our future work will focus on the modification of the EnKF with equality constraints for nonlinear MHD turbulence simulation.

References

[1] Jeffrey P Freidberg. *ideal MHD*. Cambridge University Press, 2014.

[2] Charles R Evans and John F Hawley. Simulation of magnetohydrodynamic flows-a constrained transport method. *Astrophysical Journal, Part 1 (ISSN 0004-637X), vol. 332, Sept. 15, 1988, p. 659-677.*, 332:659–677, 1988.

[3] Steven A Orszag and Cha-Mei Tang. Small-scale structure of two-dimensional magnetohydrodynamic turbulence. *Journal of Fluid Mechanics*, 90(1):129–143, 1979.

[4] Ben Snow, Andrew Hillier, Giulia Murtas, Gert JJ Botha, and Stefano Camera. Shock identification and classification in 2d magnetohydrodynamiccompressible turbulence—orszag–tang vortex. *Experimental Results*, 2:e35, 2021.

[5] Richard S Bucy. New results in linear filtering and prediction theory. *J. Basic Engrg. ASME, Ser. D*, 83:95–108, 1961.

[6] Geir Evensen. The ensemble kalman filter: Theoretical formulation and practical implementation. *Ocean dynamics*, 53:343–367, 2003.

[7] Matthew E Hubbard. Multidimensional slope limiters for muscl-type finite volume schemes on unstructured grids. *Journal of Computational Physics*, 155(1):54–74, 1999.

[8] Bruno O Soares Teixeira, Jaganath Chandrasekar, Leonardo A Borges Tôrres, Luis A Aguirre, and Dennis S Bernstein. Unscented filtering for equality-constrained nonlinear systems. In *2008 American Control Conference*, pages 39–44. IEEE, 2008.

[9] Bruno OS Teixeira, Aaron Ridley, Leonardo AB Tôrres, Luis A Aguirre, and Dennis S Bernstein. Data assimilation for magnetohydrodynamics with a zero-divergence constraint on the magnetic field. In *2008 American Control Conference*, pages 2534–2539. IEEE, 2008.